STRUCTURE AND PROPERTIES OF SURFACE LAYERS OBTAINED VIA NONVACUUM ELECTRON-BEAM CLADDING WITH COPPER AND BORON POWDER MIXTURES

K. I. Emurlaev,[1] **M. G. Golkovsky,**[2] **N. V. Stepanova,**[3] **and Z. B. Bataeva**[4]   UDC 669.017.16

Powder mixtures containing copper, boron, and iron were deposited on flat steel billets via nonvacuum electron-beam cladding to form surface layers of increased thickness. The structure, microhardness, and tribotechnical properties of the deposited materials were investigated. Eutectic colonies formed during electron-beam cladding contained iron boride frameworks filled with α-phase microvolumes. The maximum microhardness of the deposited material was approximately 500 *HV*, owing to the formation of iron boride and the release of ε-copper nanoinclusions. The obtained materials exhibited a lower friction coefficient and higher wear resistance than low-carbon steel during a sliding friction test in the presence of a lubricant. The wear resistance values recorded during sliding friction tests correlated with the microhardness levels of the deposited materials.

Keywords: nonvacuum electron-beam cladding, copper, boron, iron boride, tribotechnical properties.

Alloying steels with copper generally increases their strength properties and corrosion resistance [1–6]. However, copper is almost insoluble in ferrite at near-room temperatures and poorly soluble in steels heated to the austenitic condition; thus, the strict control of copper content in iron–carbon alloys is required [7–11]. Cuprous inclusions insoluble in austenite, characterized by a low melting point, reduce the technological properties of the alloys [12]. Crack defects are formed during the hot rolling of billets fabricated with liquid copper inclusions [13]. Liquid inclusions deformed during pressure treatment act as wedges, leading to the formation and extension of microcracks, which form macroscopic defects.

Copper can improve the tribotechnical properties of iron–carbon alloys [14, 15]. The friction coefficient of ε-copper inclusions — that is, a solid solution of copper and iron or other elements (e.g., bronze) — is considerably less than those of carbon steels [10, 16]. Studies have reported a decrease in the friction coefficient of iron–carbon alloys with increasing copper concentration [17–20]. This problem is related to the formation of surface-modified layers on steel products. Nonvacuum electron-beam cladding of steel with powder mixtures is an effective high-performance process of surface alloying [13, 21–26].

The Study Aimed to form high-thickness copper-alloyed surface layers on steels and study the structure and properties of the obtained steels.

[1] Novosibirsk State Technical University, Novosibirsk, Russia; e-mail: emurlaev@corp.nstu.ru.

[2] G. I. Budker Institute of Nuclear Physics, Siberian Branch Russian Academy of Sciences, Novosibirsk, Russia; e-mail: golkovski@mail.ru.

[3] Novosibirsk State Technical University, Novosibirsk, Russia; e-mail: stepanova@corp.nstu.ru.

[4] Siberian State University of Water Transport, Novosibirsk, Russia; e-mail: ktuk@nsawt.ru.
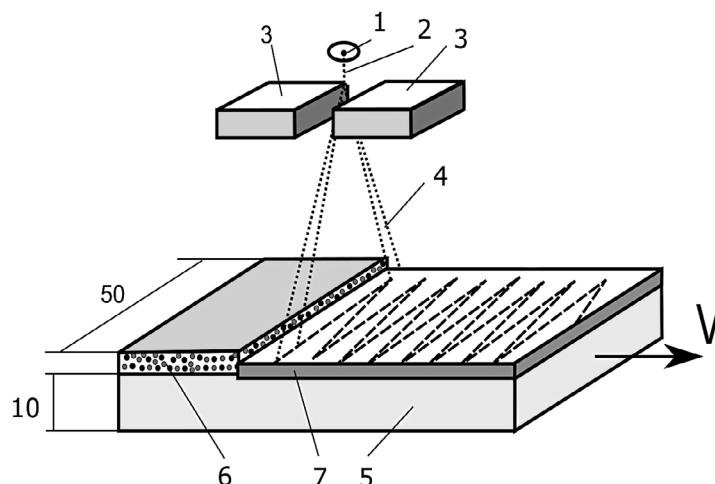
Fig. 1. Cladding steel with a powder mixture by an electron beam released into the air: *1* — electron-release device; *2* — concentrated electron beam; *3* — poles of electromagnetic scanning; *4* — scanning electron beam; *5* — steel billet; *6* — powder mixture; *7* — deposited layer.

Table 1

Composition of Materials and Modes of Nonvacuum Electron-Beam Cladding

Grade	Basic material	Alloying elements, mass.%			Flux, wt.%	Filling density, g/cm^2	Beam current, mA
		Fe	Cu	B	MgF_2		
Fe20Cu30–0.3[*]	12H18N10T	20	30	–		0.3	
Fe50Cu50	Steel 45	50	50	–			
Fe15Cu20B15	Steel 20	15	20	15	50		28
Fe10Cu30B10	Steel 10	10	30	10		0.2	
Fe10Cu35B5		10	35	5			

[*]0.3 indicates filling density.

Materials and Methods

Plates with dimensions of $100 \times 50 \times 10$ mm made of carbon steels 10, 20, 45, and alloy steel 12H18N10T were used as billets for cladding. Steel billets were clad with a powder mixture of copper (20 wt.%–50 wt.%), iron (10%–50%), amorphous boron (0%–15%), and flux MgF_2 (50%). Different filling densities were adopted: 0.2 and 0.3 g/cm^2. Iron was added to the cladding mixtures to increase the uniformity of the compositions of the alloyed surface layers. MgF_2 was used as a flux to protect the melt from oxidation. To ensure homogeneity, the cladding materials were mixed in a planetary mill for 10 min. The compositions of the cladding mixtures are presented in Table 1.

The materials were clad on an ELV-6-type electron accelerator produced by the Institute of Nuclear Physics, Siberian Branch of the Russian Academy of Sciences. The cladding scheme is presented in Fig. 1.

Steel billets clad with powder mixtures were longitudinally displaced relative to the outlet at a speed of 10 mm/s.

Under the influence of accelerating voltage, the electrons acquired a velocity close to the relativistic velocity and were released into the atmosphere through a system of diaphragms. The electromagnetic scanning system deflected the electron beam in a direction perpendicular to the sample movement. An electron beam with a frequency of 50 Hz was deflected by 25 mm to one side and the centerline of the sample. The electron-beam energy was 1.4 MeV. Steel billets were positioned at 90 mm from the outlet. The diameter of the electron beam on the surface processed was 12 mm. The powder mixture was deposited at an electron beam current of 28 mA, which corresponded to an energy density of 7.84 kJ/cm^2.

The structures of the materials deposited were studied via light microscopy, scanning electron microscopy, and transmission electron microscopy, using Carl Zeiss Axio Observer Z1 m, Carl Zeiss EVO 50 XVP, and FEI Tecnai G2 20 TWIN microscopes. The scanning electron microscope was equipped with an Oxford Instruments X-Act energy-dispersive X-ray spectrometer for energy-dispersive X-ray spectroscopy analysis (EDX). Phase analysis was performed on an ARL X'TRA θ-θ diffractometer. The X-ray source was a copper X-ray tube (voltage 45 kV, current 35 mA), with a wavelength (λ) of 1.5406 Å. Diffraction patterns were obtained using the Bragg–Brentano geometry. Diffraction patterns were recorded in a step-by-step mode $(\Delta 2\theta = 0.05\,°;\ t = 5–12\ \text{s})$. The phases present in the studied materials were identified according to the ICDD PDF-4 database.

The microhardness of the deposited layers was measured on transverse sections using a Wolpert Group 402MVD device. The load on the diamond indenter in the form of a tetrahedral pyramid was 0.98 N. The indenter prints were applied from the sample surface to the base metal. The sliding friction coefficient was determined using an SMT-1 friction machine during the "disk–plane" scheme. During the tests, mineral oil was fed into the friction zone. The loads on the samples in all cases were the same $(P = 1000\ \text{N})$, the rotation frequency was 200 min^{-1}, and the total test time was 180 min (9 cycles of 20 min). Moreover, 50 mm-diameter disks made of *HRC* 55 hardened steel 45 were used as counterbodies. The wear resistance of the materials was assessed according to the volume of the worn material, which was calculated from the wear hole parameters. The base material (i.e., low-carbon steel 10) was used as a reference.

Results and Discussion

Surface Alloying of Steels of Various Compositions. At stage 1, the formation of deposited layers of powder mixtures of copper and iron on unalloyed steel billets containing 0.1%, 0.2%, and 0.45% carbon and chromium–nickel steel (12H18N10T) was experimentally analyzed. During the cladding, approximately 70% of the electron-beam energy was released in the powder filling, and the remaining 30% was used to melt the base material. The results of structural studies indicated that regardless of the base metal composition (substrate), transverse cracks were formed in the copper-alloyed layers (Fig. 2). The crack formation was related to the difference in the values of the temperature coefficients of the linear expansions of copper and steel.

To prevent crack formation on the alloyed surface layers, boron powder and copper were introduced into the cladding mixture. The formation of a eutectic of the $(\alpha\text{-Fe–Fe}_2\text{B})$ type, with a crystallization temperature of 1174 °C, will bring the crystallization temperature of the iron-containing melt closer to that of copper (1085 °C). The amounts of flux in all experiments were equal (i.e., 50% of the mass of the powder filling). The boron, copper, and iron contents were varied in the ranges of 5 wt.%–15 wt.%, 20%–35%, and 10%–15%, respectively. Technological experiments showed that the addition of amorphous boron to the powder filling suppressed crack formation in the layers deposited. No major defects were observed in the surface zones and at the boundaries of material fusion.
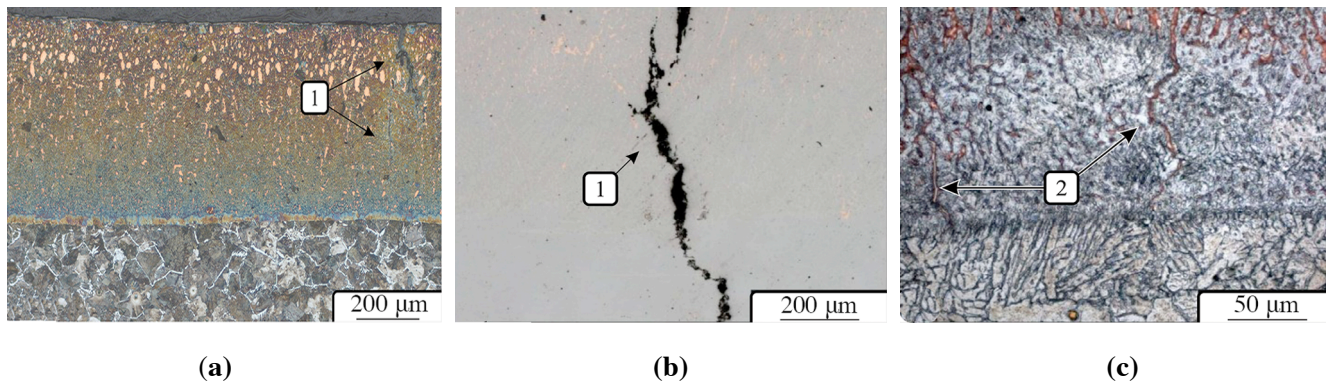
Fig. 2. Structure of the deposited layers with cracks, obtained through the deposition of copper and iron powder mixtures on steel 45 (a) and 12H18N10T (b), (c) via nonvacuum electron-beam cladding: *1* — cracks; *2* — copper-filled cavities.
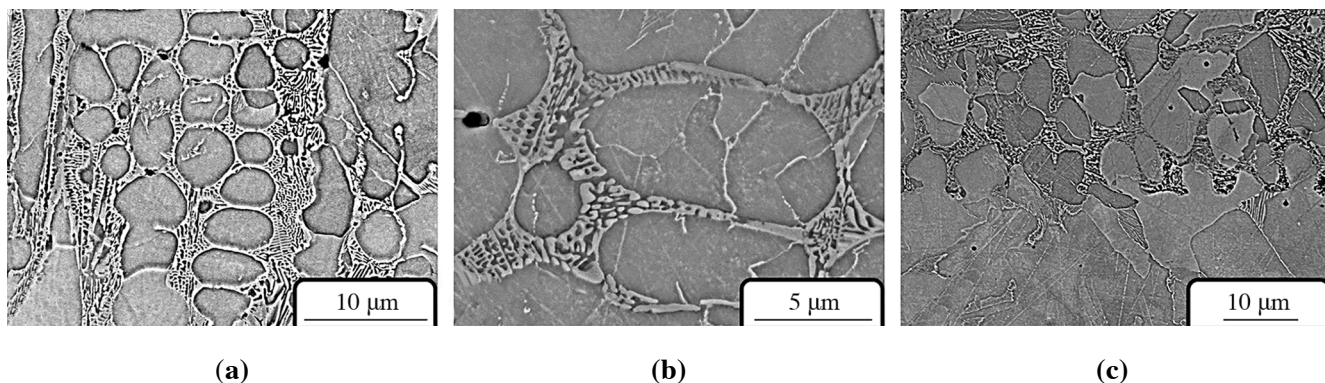

Fig. 3. Thin structure of the layer formed via nonvacuum electron-beam cladding of low-carbon steel billets with copper, boron, and iron: (a), (b) — hypoeutectic structure in the middle of the deposited layer; (c) — structure of the transition zone between the base metal and coating.

Structure of the Surface Layers Obtained Through Electron-Beam Deposition of Fe–Cu–B Powder Mixtures. A heterophase layer was formed during the deposition of Fe–Cu–B powder mixtures. The middle zones of the deposited layers contained colonies of the "α-Fe–Fe$_2$B" eutectic and microvolumes of alpha-iron, with evenly distributed ε-Cu particles. The surface layers, which were least diluted with iron, exhibited the maximum content of alloying elements. In these zones, along with the eutectic colonies, isolated crystals of iron borides of various shapes were observed. The volume fraction of the eutectic decreased toward the cladding boundary.

Figures 3a and b show images of the hypoeutectic composition zone obtained via scanning electron microscopy. The boundaries formed during nonvacuum electron-beam cladding (Fig. 3c) exhibited a clear transition from the deposited layer to base metal (low-carbon steel). Small isolated pores occurred, but microcracks were not formed. A high-quality bond existed between the deposited layers and the base metal.

Figure 4a presents the transmission electron microscopy image of the eutectic. The base of the colony is represented by a boride framework. The cavities in the colony were filled with alpha-iron. The distance between the rounded and elongated microvolumes of α-Fe was approximately 100–200 nm. According to Bataev et al. [21], rounded precipitates in the Fe–B system represent former regions of delta ferrite. Upon subsequent cooling of the material, the δ-ferrite was transformed into the γ-phase and then the α-phase. Excess boron could be separated from the analyzed areas, and a eutectoid of lamellar morphology was formed.
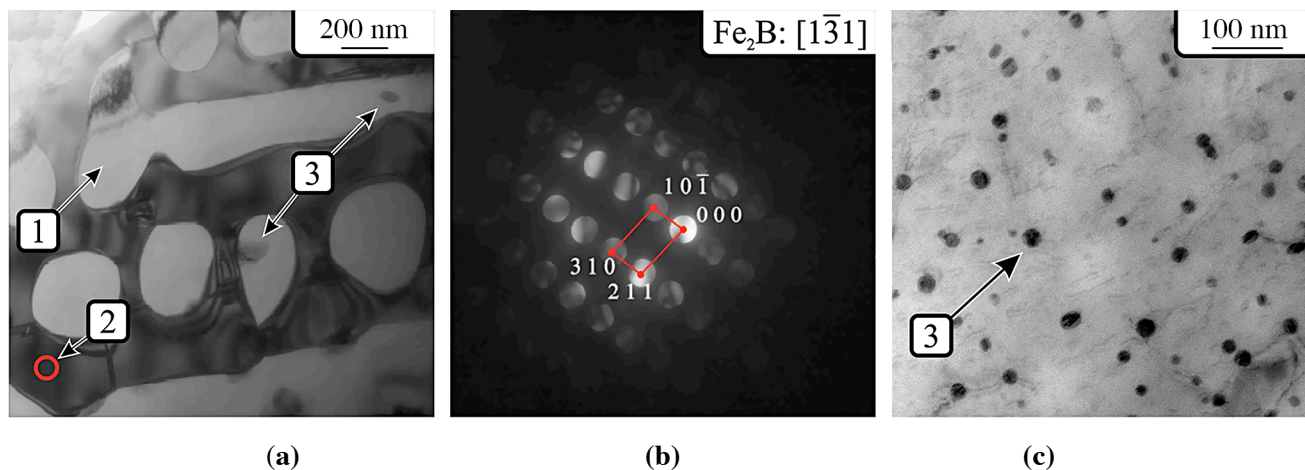
Fig. 4. Structure of the deposited layer, determined via transmission electron microscopy: (a) — eutectic "α-Fe–Fe$_2$B"; (b) — electron diffraction patterns with a highlighted zone circumference; (c) — ε-Cu particles in the alpha-iron structure; *1* — α-Fe; *2* — zone corresponding to the diffraction pattern (b); *3* — ε-Cu particles.

According to the EDX analysis results, the deposited coatings of Fe15Cu20B15, Fe10Cu30B10, and Fe10Cu35B5 samples contained 3%–5% copper. The copper content of the surface layer was considerably less than that of the cladding mixture because of several factors, one of which is associated with the dilution of alloying elements in the melt of the surface layers of steel billets. Part of the copper was removed from the cladding mixture in the form of splashes during the accelerated heating of the material by an electron beam. Moreover, part of the copper in the alloyed surface layers evaporated owing to the intense heating of the powder mixture.

Under equilibrium conditions, copper is almost insoluble in α-iron [7, 10]. However, the conditions for the formation of alloy structures during nonvacuum electron-beam cladding with powder mixtures were far from equilibrium. Thus, some of the copper in the alloyed surface layer existed as a metastable solid solution, while the rest was released as ε-copper nanoparticles evenly distributed in the alpha-iron. The particle size did not exceed 20 nm (Fig. 4c). Cast iron–copper alloys in a previous study revealed a similar structure [13]. However, the layer deposited by an electron beam exhibited a greater dispersion of ε-Cu particles than the cast alloy, which is due to the increased cooling rate of the deposited layer, characteristic of the electron-beam cladding technology.

Phase Composition of Deposited Materials. The phase composition of the deposited layers was analyzed via X-ray diffractometry. Fe$_2$B boride and α-phase were found in the layers, regardless of the compositions of the deposited mixture and deposited layer (Fig. 5).

Results of Tribotechnical Studies of Alloyed Surface Layers. The behavior of the surface layers under sliding friction in the presence of a lubricant was analyzed. The steel clad with a mixture of copper, boron, and iron exhibited considerably higher wear resistance than the base material (steel 20) (Fig. 6). During the tests, which lasted 180 min, a 1.42 mm^3 hole was formed on the base metal sample. Only 0.022 mm^3 of the alloyed surface material Fe15Cu20B15 was worn out under similar friction conditions. The wear resistance of the material deposited was considerably greater than that of the low-carbon steel owing to the formation of high-strength particles of iron boride (Fe$_2$B) on the surface-hardened layer. The introduction of alloying elements into the alloy also reduced the friction coefficient from 0.12 to 0.09, which is related to the favorable influence of ε-copper nanoparticles in the α-phase.
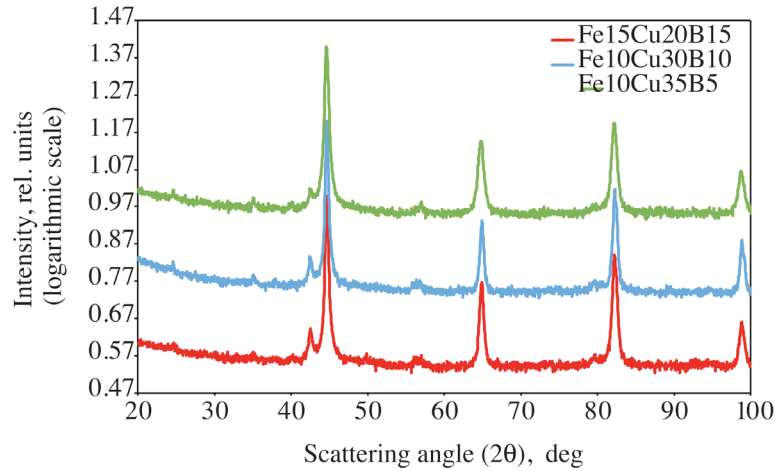
**Fig. 5.** Results of X-ray phase analysis of deposited layers Fe15Cu20B15, Fe10Cu30B10, and Fe10Cu35B5.
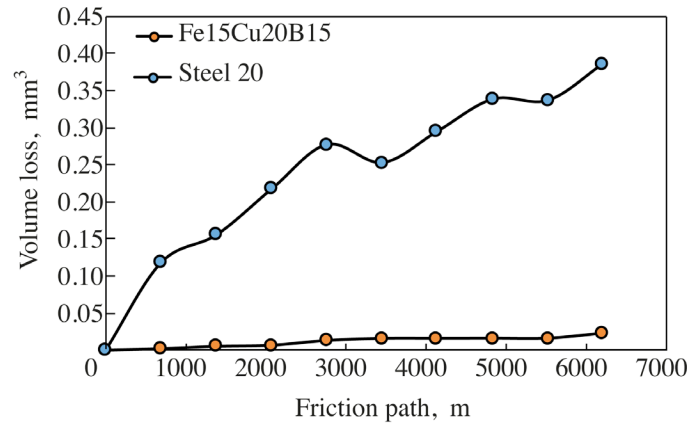
Fig. 6. The change in the material volume lost during the testing of steel 20 and alloy Fe15Cu20B15 samples according to the "disk–plane" scheme.

Microhardness of Deposited Materials. The dependencies presented in Fig. 7 indicate that the depth of the alloyed surface layers ranged from ≈ 2500 to ≈ 3000 μm and depended on the composition and amount of the mixture deposited. The Fe10Cu30B10 alloy specimens exhibited the maximum values of microhardness ($\approx 500\ HV$). The Fe10Cu35B5 samples exhibited close results. The average microhardness of these layers (≈ 450–$460\ HV$) was approximately three times that of the base metal ($\approx 160\ HV$). The microhardness varied because the diamond indenter fell on different parts of the alloyed heterophase surface layer when straight prick lines were applied. The peak microhardness values corresponded to microvolumes with higher iron boride proportion. The measurement results were probably influenced by both the spatial orientation and size of the crystals. The lowest microhardness values corresponded to areas with higher proportions of the low-strength α-phase.

CONCLUSIONS

Powder mixtures of copper and amorphous boron were deposited on flat billets of low-carbon steel via nonvacuum electron-beam cladding to obtain surface-hardened layers with up to ≈ 3 mm thickness. The maximum
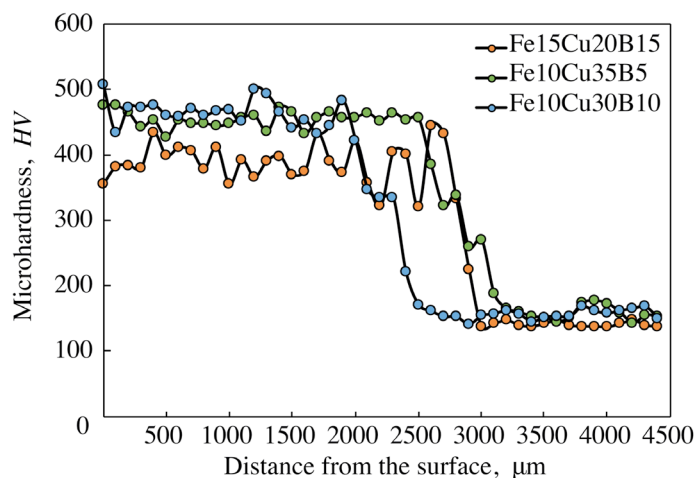
Fig. 7. Distribution of microhardness in the cross section of samples obtained through the deposition of a mixture of copper, boron, and iron on low-carbon steel.

microhardness of surface-alloyed materials reached ≈ 500 HV. The main structural factors responsible for the increased strength of the clad materials were the presence of a eutectic based on iron and boron, and ε-copper nanoinclusions. The deposited layers consisted of an α-Fe–Fe$_2$B eutectic and α-Fe volumes with uniformly distributed ε-Cu nanoparticles. Eutectic colonies formed during electron-beam cladding consisted of iron boride frameworks with microvolumes of the α-phase. The tribotechnical properties of the deposited materials surpassed those of low-carbon steels. The wear resistance of the surface-hardened layers under sliding friction in the presence of a lubricant correlated with their hardness. The friction coefficient of the weld metal was considerably less than that of low-carbon steel.

REFERENCES

1. D. M. Buck, "Copper in steel: the influence on corrosion," *J. Ind. Eng. Chem.*, **5(6)**, 447–452 (2013).
2. B. Li, H. Qu, and Y. Lang, "Copper alloying content effect on pitting resistance of modified 00Cr20Ni18Mo6CuN super austenitic stainless steels," *Corros. Sci.*, **173**, Art. 108791 (2020).
3. X. Y. San, B. Zhang, B. Wu, X. X. Wei, E. E. Oguzie, and X. L. Ma, "Investigating the effect of Cu-rich phase on the corrosion behavior of Super 304H austenitic stainless steel by TEM," *Corros. Sci.*, **130**, 143–152 (2018).
4. Z. X. Zhang, G. Lin, and Z. Xu, "Effects of light predeformation on pitting corrosion resistance of copper-bearing ferrite antibacterial stainless steel," *J. Mater. Process. Technol.*, **205**, 419–424 (2008).
5. S. Jeon, S. Kim, I. Lee, J. Park, K. Kim, J. Kim, and Y. Park, "Effects of copper addition on the formation of inclusions and the resistance to pitting corrosion of high Performance duplex stainless steels," *Corrosion Science*, **53**, 1408–1416 (2011).
6. J. Zhang and D. J. Young, "Effect of copper on metal dusting of austenitic stainless steels," *Corros. Sci.*, **49**, 1450–1467 (2007).
7. K. Shubhank and Y. Kang, "Critical evaluation and thermodynamic optimization of Fe–Cu, Cu–C, Fe–C binary systems and Fe–Cu–C ternary system," *Comput. Coupling Ph. Diagr. Thermochem.*, **45**, 127–137 (2014).
8. G. I. Silman, V. V. Kamynin, and V. V. Goncharov, "The mechanisms of the influence of copper on the formation of structure in cast iron," *MiTOM*, No. 9, 16–22 (2007).

9. G. I. Silman, V. V. Kamynin, and A. A. Tarasov, "Effect of copper on structure formation in cast iron," *Met. Sci. Heat Treat.*, **45**, No. 7-8, 254–258 (2003).

10. S. Upadhyay and K. K. Saxena, "Effect of Cu and Mo addition on mechanical properties and microstructure of gray cast iron: An overview," *Mater. Today: Proc.*, **26**, Part 2, 2462–2470 (2020).

11. H. Sazegaran, F. Teimoori, H. Rastegarian, and A. M. Naserian-Nik, "Effects of aluminum and copper on the graphite morphology, microstructure, and compressive properties of ductile iron," *J. Min. Metall., Sect. B Metall.*, **57**, B. 1, 145–154 (2021).

12. I. Le May and L. M. -D. Shetki, *Copper in Ferrous Metals* [in Russian], ed. O. A. Bannykh, Metallurgiya, Moscow (1988).

13. D. V. Lazurenko, G. I. Alferova, K. I. Emurlaev, Y. Y. Emurlaeva, I. A. Bataev, T. S. Ogneva, A. A. Ruktuev, N. V. Stepanova, A. A. Bataev et al., "Formation of wear-resistant copper-bearing layers on the surfaces of steel substrates by non-vacuum electron beam acladding using powder mixtures," *Surf. Coat. Technol.*, **395**, Art. 125927, 14 (2020).

14. W. Osterle, C. Prietzel, H. Kloss, and A. I. Dmitriev, "On the role of copper in brake friction materials," *Tribol. Int.*, **43**, 2317–2326 (2010).

15. I. A. Bataev, N. V. Stepanova, A. A. Bataev, A. A. Nikulina, and A. A. Razumakov, "Aspects of isolation of nanosized particles of ε-phase of copper in ferrite gaps of lamellar pearlite," *Fiz. Metall Metalloved.*, **117**, No. 9, 932–937 (2016).

16. L. N. Garcia, A. J. Tolley, F. D. Carazo, and R. E. Boeri, "Identification of Cu-rich precipitates in pearlitic spheroidal graphite cast irons," *Mater. Sci. Technol.*, **35**, B. 18, 2252–2258 (2019).

17. J. O. Agunsoye, S. A. Bello, S. B. Hassan, R. G. Adeyemo, and J. M. Odii, "The effect of copper addition on the mechanical and wear properties of gray cast iron," *J. Miner. Mater. Character. Eng.*, **2**, 470–483 (2014).

18. B. Zhang, B. Xu, and Yi. Xu, "Cu nanoparticles effect on the tribological properties of hydrosilicate powders as lubricant additive for steel-steel contacts," *Tribol. Int.*, **44(7)**, 878–886 (2011).

19. W. Zhai, W. Lu, and X. Liu, "Nanodiamond as an effective additive in oil to dramatically reduce friction and wear for fretting steel/copper interfaces," *Tribol. Int.*, **129**, 75–81 (2019).

20. A. C. P. Rodrigues, W. Oesterle, and T. Gradt, "Impact of coppernanoparticles on tribofilm formation determined by pin-on-disc tests with powder supply: Addition of artificial third body consisting of Fe_3O_4, Cu and graphite," *Tribol. Int.*, **110**, 103–112 (2017).

21. I. A. Bataev, M. G. Golkovskii, A. A. Losinskaya, A. A. Bataev, A. I. Popelyukh, T. Hassel, and D. D. Golovin, "Non-vacuum electron-beam carburizing and surface hardening of mild steel," *Appl. Surf. Sci.*, **322**, 6–14 (2014).

22. M. Eroglu, "Boride coatings on steel using shielded metal ARC welding electrode: microstructure and hardness," *Surf. Coat. Tech.*, **203**, 2229–2235 (2009).

23. O. Lenivtseva, I. Bataev, M. Golkovski, A. Bataev, V. Samoilenko, and N. Plotnikova, "Structure and properties of titanium surface layers after electron beam alloying with powder mixtures containing carbon," *Appl. Surf. Sci.*, **355**, 320–326 (2015).

24. D. V. Lazurenko, I. S. Laptev, I. Bataev, A. A. Ruktuev, C. Gollwitzer, et al., "Influence of the Ti/Al/Nb ratio on the structure and properties on intermetallic layers obtained on titanium by non-vacuum electron beam cladding," *Mater. Character.*, **163**, Art. 110246, 13 p. (2020).

25. D. A. Santana, G. Y. Koga, W. Wolf, I. A. Bataev, A. A. Ruktuev, C. Bolfarini, C. S. Kiminami, W. J. Botta, and A. M. Jorge, "Wear-resistant boride reinforced steel coatings produced by non-vacuum electron beam cladding," *Surf. Coat. Tech.*, **386**, Art. 125466 (2020).

26. T. A. Krylova and Yu. A. Chumakov, "Fabrication of Cr–Ti–C composite coating by non-vacuum electron beam cladding," *Mater. Lett.*, **274**, Art. 128022 (2020).